Journal of Environmental Chemical Engineering 6 (2018) 3070–3082

Contents lists available at ScienceDirect

Journal of Environmental Chemical Engineering

journal homepage: www.elsevier.com/locate/jece

Conversion of waste tire rubber into a high-capacity adsorbent for the removal of methylene blue, methyl orange, and tetracycline from water

Md. Tariqul Islam[a,b], Ricardo Saenz-Arana[a], Cesar Hernandez[a], Thomas Guinto[a], Md Ariful Ahsan[a], Dwayne T. Bragg[a], Huiyao Wang[c], Bonifacio Alvarado-Tenorio[d,*], Juan C. Noveron[a,b,*]

[a] Department of Chemistry, University of Texas at El Paso, 500 West University Avenue, El Paso, TX, 79968, USA
[b] NSF Nanosystems Engineering Research Center for Nanotechnology Enabled Water Treatment (NEWT), USA
[c] CURRL, New Mexico State University, 945 College Drive, Las Cruces, USA
[d] Instituto de Ciencias Biomédicas, Universidad Autónoma de Ciudad Juárez, Ciudad Juárez, Chihuahua, Mexico

ARTICLE INFO

Keywords:
Adsorption
Methyl orange
Methylene blue
Tetracycline
Waste tire rubber
Sulfonation

ABSTRACT

There has been growing interest in making adsorbents more cost-effective and feasible in low resource areas by using material that is cheap or would usually be considered waste. In the present study, a high-capacity regenerable adsorbent is synthesized by the treatment of waste tire rubber (WTR) with concentrated sulfuric acid. The sulfuric acid reflux carbonized as well as functionalized the WTR with the sulfonic acid group. The as-prepared sulfonated carbonaceous WTR was used for the removal of organic dyes and antibiotic viz. methylene blue (MB), methyl orange (MO) and Tetracycline (TC) from water. The maximum adsorption capacity was found to be about 833, 588, and 303 mg/g towards MB, MO, and TC, respectively. The adsorption of MB, MO, and TC from the tap water matrix was also performed and shown to maintain similar adsorption capacities as the deionized water. In addition, a packed glass column was prepared to demonstrate the continuous adsorption of MB and TC from the tap water matrix. The regeneration of the column was achieved by using mixture of aqueous and organic solvents with dissolved NaOH and it was demonstrated that the adsorbent not only recovered but also increased its adsorption capacity after every time it was regenerated.

1. Introduction

Due to the rapid growth of the automobile industry, the disposal of the waste tire rubber (WTR) has become an emergent threat worldwide and there are tons of it being piled up every day. According to a study reported in 2001, approximately 800 million waste tires are disposed around the world per year [1]. This amount is predicted to increase by approximately 2% each year. The WTR, consisting of styrene-butadiene polymer and others, is extremely resistant to the natural degradation [2]. Moreover, the WTR has no such important applications, although there are some reports of their utilization for environmental remediation [3–5], catalysis [6,7], energy storage [8–10], etc. Therefore, the recycle and reuse of the WTR could be beneficial economically as well as environmentally. Along the same line, the population growth and increased industrialization are leading to a global scarcity of water at many levels. Therefore, in the clean water sector, water contamination with organic and inorganic pollutants is becoming a serious health concern in both rural and urban areas [11].

In this regard, preparation of high-capacity and cost-effective adsorbent out of WTR for the wastewater treatment could be a lucrative choice both economically and green chemistry point of view. The utilization of WTR for water treatment may provide twofold benefits. Firstly, the WTR, which is considered as a waste, could find a useful application with due economic value. Secondly, its utilization for the remediation of environmental pollutants from the water may provide the access to clean water for the people in resource-limited areas.

Traditional adsorbents, for the removal of the organic pollutants from water such as activated carbon or charcoal, are difficult to produce as well as functionalize into new materials. Although activated charcoals are very efficient for the removal of organic pollutants in water their ability for the removal of heavy metals ions and ionic organic pollutants is limited. Thus the development of new polymeric adsorbents with multifunctional components that may uptake organic and inoragnic pollutants by π-π stacking, hydrogen bonding, and electrostatic interactions would pave the way to more effective adsorbents in the future.

* Corresponding authors at: Department of Chemistry, University of Texas at El Paso, 500 West University Avenue, El Paso, TX, 79968, USA.
E-mail addresses: bonifacio.alvarado@uacj.mx (B. Alvarado-Tenorio), jcnoveron@utep.edu (J.C. Noveron).

https://doi.org/10.1016/j.jece.2018.04.058
Received 19 January 2018; Received in revised form 26 March 2018; Accepted 23 April 2018
Available online 25 April 2018
2213-3437/

Scheme 1. Preparation of sulfonated waste tire rubber (WTR-SO_3H) and the possible structure of the pristine styrene-butadiene polymer and the sulfonated styrene-butadiene polymer.

In the present study, a high-capacity multifunctional and regenerable adsorbent is synthesized by treating the WTR with concentrated sulfuric acid. The WTR was used as the base material in this study knowing that the tire rubber consists of styrene-butadiene polymer [12], which could easily be sulfonated and carbonized by the treatment with sulfuric acid. The carbonaceous sulofanted waste tire rubber (WTR-SO_3H) was used for the removal of emerging pollutants such as methylene blue (MB), methyl orange (MO) and Tetracycline (TC) from the water. MB and MO were used because they are widely used in numerous industries and known to have harmful effects on the living organisms and the whole ecosystem [13]. They are also known to have high resistance to natural degradation. On the other hand, TC is a broadband antibiotic, which has a widespread application in cattle and poultry industries and their disposal in water is posing a new type of threat to the environment [14,15]. The presence of antibiotic in the environment is unexpected and they gradually make the microorganisms more resistant to drug. Therefore, like other pollutants, the removal of antibiotics is an essential part of wastewater treatment. The adsorption capacity of the WTR-SO_3H was tested by realizing multiple batch experiments where different variables, such as pH, temperature, the concentration of pollutants, were controlled and measured. The adsorption of MB, MO, and TC from tap water matrix was also evaluated and shown to maintain similar adsorption capacity as in the deionized water. In addition, a packed glass column was prepared to demonstrate the continuous adsorption of MB and TC from the tap water matrix.

2. Experimental section

2.1. Materials

Metal wire stripped off ground waste tire rubber was obtained from a local tire recylying shop (Cd. Juarez, Mexico). Concentrated sulfuric acid (95–98%), sodium hydroxide (> 97%), acetone (> 99.5%), and reagent alcohol (Ethanol = 72–73%) were purchased from BDH Chemicals. Methyl orange (> 95%) and methylene blue (> 98%) were obtained from AMRESCO Ltd. and Consolidated Chemical, respectively. Tetracycline (≥98%) was purchased from Sigma Aldrich. Coarse sand was purchased from J.T. Baker (CAS Number: 14808-60-7, MDL No. MFCD02100519). Ultrasonic batch sonicator (VWR 50T) was used to homogenize the adsorption mixture. Quartz cuvette having volume of 4 mL and path length of 10 mm was used for the UV–vis studies. Deionized water with a resistance of about 18.2 MΩ cm at 25 °C was obtained from Milli-Q water purifier facilities (EMD Millipore Corporation) from the lab. Tap water was obtained from the regular water faucet of the lab. The complete list of the soluble and insoluble species of the tap water is given in Supporting information, Fig. S1.

2.2. Preparation of the sulfonated waste tire rubber (WTR-SO_3H)

The sulfonation of the WTR is depicted in Scheme 1. In detail, in a 300 mL round bottomed flask, 5 g of the ground WTR was mixed with 40 mL of concentrated H_2SO_4 (95–98%). Excess of H_2SO_4 was used to obtain a good suspension of the WTR in the acid so that it could be stirred during the reflux. The mixture was refluxed in boiling H_2SO_4 for 3 h while stirring. During the reflux, it was observed that the solution expanded like foam to a certain point, and then settled back to its original volume after approximately an hour of reflux. Once the reflux finished, the reaction mixture was cooled down to room temperature and 250 mL of ice-cold water was slowly added to the mixture with due precautions. Afterwards, the product was filtered by vacuum filtration and washed with deionized water to remove any excess H_2SO_4. The sulfonated waste tire rubber was then dried in vacuum oven at 65 °C for 12 h. After the adsorbent had fully dried, it was ground to a fine powder by use of a ceramic mortar and pestle. The amount of the WTR-SO_3H was approximately 4.7 g.

2.3. Batch adsorption experiments

For the batch adsorption of MO and TC, 10 mg of the WTR-SO_3H was added into 20 mL solution of the MO and TC having initial concentrations varying from 50 to 400 ppm. Then, the mixtures were bath sonicated for 30 min, which was followed by 24 h of stirring at 1000 rpm on a magnetic stirring plate. The time-dependent adsorption studies revealed that the adsorption of MB, MO, and TC reached to equlibrium after 24 h of stirring. Therefore, the stirring period of 24 was used for all the equilibrium adsorption studies. After 24 h of stirring, 1 mL of the mixture was filtered through a 0.25 μm PTFE syringe filter to obtain a clear filtrate. The adsorption capacity was calculated from the difference between the initial and final concentration of the MO and TC, which was obtained by using UV–vis spectrophotometer. The concentrations of the MO and the TC were obtained from their abosrbance at 464 and 357 nm, respectively [16,17]. For the batch adsorption of MO and TC, acidic pH was chosen because the pH-dependent studies revealed that the adsorption of MO and TC was highly favored in the acidic pH.

The batch adsorption of MB was carried out following the same experimental procedure. The only difference was the amount of

adsorbent viz. 20 mg. Moreover, the adsorption of MB was carried at the pH of 3.5, 7, and 10 to determine the equilibrium adsorption capacities at the acidic, neutral, and basic pH. The adsorption capacity was calculated from the difference between the initial and final MB concentrations, which was determined from the absorbance of MB centered at 615 nm by using the UV–vis spectroscopy [18].

The pH-dependent adsorption of MB was performed by dispersing 20 mg of the WTR-SO_3H in 20 mL of 700 ppm MB solutions. In case of the pH-dependent adsorption of MO and TC, 10 mg of the adsorbent was dispersed in 20 mL of 100 ppm and 200 ppm of MO and TC solutions, respectively. The pH of the solution was adjusted by using 1 M NaOH and 1 M HCl solutions.

The time-dependent adsorption capacity was obtained by adding 20 mg of the WTR-SO_3H in 40 mL of 200 ppm MB solution at pH ~ 7. For the time-dependent adsorption of MO and TC, 10 mg of the adsorbent was added in 20 mL of 100 ppm MO and 50 ppm TC solutions at pH ~ 3.6. Acidic pH (~3.6) was choosen as it was found that the adsorption of MO and TC was favored in acidic pH. Bath sonication was carried out for 30 min and while sonication samples (~0.5 mL) were taken at every 10 min time interval. After the bath sonication, the mixture was stirred continuously on a magnetic stirring plate at 1000 rpm and during which samples were taken at every 30 min interval.

The temperature-dependent adsorption studies were performed using 10 mg of the adsorbent in 20 mL of the MB and MO solution at 23, 40, and 60C. pH 10 and 3.6 were chosen for the adsorption of MB and MO respectively. It was found that the TC decomposed at elevated temperature (e.g 60 °C) and thereby the temperature-dependent adsorption of TC was not perfermoed under our experimental conditions.

2.4. Preparation of the adsorption column

A fritted chromatographic column with reservoir having the dimensions of I.D. × L = 26 × 457 mm was packed to about 14 cm with the mixture of WTR-SO_3H and sand, Scheme 2. In detail, 2 g of the sulfonated waste tire rubber was homogeneously mixed with 105 g of sea sand by a ceramic mortar and pestle for few minutes of gentle grinding. 105 g of sand was used to achieve a good column height so that the adsorbates have good contact while passing through the column. Afterwards, the column was filled by the dry filling method. To help distribute the flow as well as to prevent the leakage of any adsorbent, cotton and coarse sea sand were used at the bottom and the top of the column, respectively.

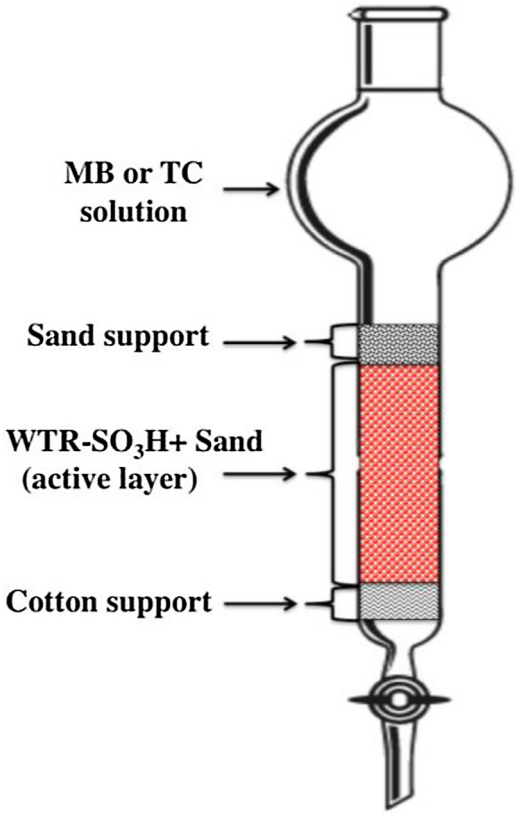

Scheme 2. Composition of the column filter packed with ST-SO H and sand for the continuous adsorption of MB and TC.

The column was first washed with 100 mL of DI water before running any adsorption cycle. For the continuous adsorption of MB, 20 ppm MB solution in tap water matrix was used without the adjustment of the pH. The solution was manually-fed into the column and allowed to pass under the gravity. The flow rate varied from 6 to 6.8 mL/min After every 1000 mL of the solution was filtered, 2 mL of filtrate was sampled for UV–vis analysis. As soon as a trace of dye was detected in the filtered water, the filtration was discontinued and the column was regenerated. The efficient regeneration of the column was achieved by using a 0.025 M NaOH solution in 99:1 reagent alcohol and water mixture. After the regeneration cycle, the column was washed with about 100 mL DI water before starting the following cycle of adsorption.

As the TC and MO demonstrated samilar kinetic and pH-dependent adsorption trend in the batch test and since TC is considered a good representative of water-soluble pharmaceutical contaminants, we utilized TC for the continuous adsorption in the column. For the continuous adsorption of TC, a separate column was made following the above-mentioned method and 10 ppm TC solution in tap water was used as the feed solution. The first cycle of adsorption was carried out without any adjustment in the pH. However, the second cycle was carried out at pH ~3.5 as the batch adsorption studies suggested that the adsorption of TC is favored in acidic pH. The regeneration of the TC filtration column was performed by using a 0.025 M NaOH solution in 50:50 acetone and water mixture.

2.5. Adsorption isotherms and adsorption kinetics

The equilibrium and time-dependent adsorption capacities were calculated using the following equations:

$$\text{Equilibrium adsorption capacity, } Q_e = \frac{C_0 - C_e}{m} \times V \quad (1)$$

The percent dye adsorption was calculated using the following equation:

$$\text{Time} - \text{dependent percent adsorption, Qt} = \frac{C_0 - C_t}{C_0} = \frac{A_0 - A_t}{A_0} \times 100\% \quad (2)$$

where C_0, C_t, and C_e represent the concentrations of the adsorbates (mg/L) at the beginning, at time t, and at the equilibrium, respectively; A_0 and A_t represent the absorbance of the adsorbates at concentrations C_0 and C_t, respectively; Q_e and Q_t represent the adsorption capacities at the equilibrium and at time t, respectively; m represents the mass of the adsorbent (g) and V represents the volume of dye solution (L).

The batch adsorption results were analyzed by utilizing the linear form of the Langmuir, Freundlich, amd the Temkin isotherm models. The Langmuir isotherm is often utilized to describe the adsorption of a solute from a liquid solution. It is based on the monolayer adsorption of molecules on the adsorbent. It assumes that the adsorption energy of each adsorbate molecule is the same, independent of the surface of the adsorbent, the adsorption takes place only on some sites and there are no interactions between the adsorbate molecules [19] . The Freundlich isotherm, on the other hand, is based on both the monolayer and multilayer adsorptions of molecules on the adsorbent [20]. The Temkin isotherm is based on the assumption that the fall in the heat of

adsorption is linear rather than logarithmic and is excellent for predicting the gas phase equilibrium [21,22]. The linear form of the Langmuir, Freundlich, and the Temkin isotherm models of adsorption are expressed by the following equations [23–25].

$$\textit{Langmuir isotherm}, \frac{C_e}{Q_e} = \frac{1}{Q_m}C_e + \frac{1}{K_L Q_m} \quad (3)$$

$$\textit{Freundlich Isother}, \ln Q_e = \frac{1}{n}\ln C_e + \ln K_F \quad (4)$$

$$\textit{Temkin Isotherm}, Q_e = B(\ln A) + B(\ln Ce) \quad (5)$$

where C_e represents the equilibrium concentrations of the adsorbates (mg/L) and Q_m represents the maximum adsorption capacities (mg/g); K_L stands for the Langmuir constant (L/mg), which is related to the affinity of the binding sites; K_F stands for the Freundlich constant (L/mg) and 1/n is defined as the exponent of non-linearity (mg/L) for a given adsorbate and adsorbent at a particular temperature. K_F and 1/n are related to the sorption capacity and the sorption intensity of the system, respectively. With the increse in the value of K_F, the adsorption capacity increases and vice-versa. On the other hand, the magnitude of 1/n gives an indication of the favorability of the sorbent-adsorbate systems. The higher the 1/n value, more favorable is the adsorption and vice-versa [26]. A and B are Temkin isotherm constants, which can be determined from the intercept and slope of linear plot of Q_e versus ln C_e, respectively [27].

The time-dependent adsorption results were analyzed by utilizing the linear form of the pseudo-first order, pseudo-second order, intra-particle diffusion, and the Elovich kinetic models, which are expressed by the following equation [28–30].

$$\text{Pseudo} - \text{second} - \text{order kinetic model}, \frac{t}{Q_t} = \frac{t}{Q_e} + \frac{1}{K_2 Q_e} \quad (6)$$

$$\textit{Pseudo} - \textit{first} - \textit{order kinetic model}, \log(Q_e - Q_t) = \log Q_e - \frac{K_1 t}{2.303} \quad (7)$$

$$\textit{Intra} - \textit{particle diffusion kinetic model}, Q_t = \frac{Kw}{w} t^{1/2} \quad (8)$$

$$\textit{Elovich kinetic model}, Q_t = \frac{1}{\beta}\ln \alpha\beta + \frac{1}{\beta}\ln(t) \quad (9)$$

where Q_e and Q_t represent the adsorption capacities (mg/g) at equilibrium and at time t (min); K_1 (1/min) and K_2 [g/(mg min)] are the rate constants of adsorption of the pseudo-first-order and pseudo-second-order kinetic models, respectively. Where w is the weight of adsorbent per volume of solution (g/L), K_W is the Weber intraparticle diffusion coefficient ($mg\,L^{-1}\,min^{-1/2}$); α is the initial adsorption rate (mg/g min) and β is the desorption constant (g/mg), which can be determined from the slope and the intercept of the Q_t vs. ln(t) plot.

3. Results and discussion

3.1. Characterization of the adsorbent

The WTR-SO_3H was physically and chemically characterized by Scanning Electron Microscopy (SEM) image, Energy Dispersive X-ray spectroscopy (EDS), X-ray photoelectron spectroscopy (XPS), Fourier Transform Infrared Spectroscopy (FTIR), Raman spectroscopy, X-ray powder diffraction (XRPD), Thermogravimetric analysis (TGA), and zeta potential measurements.

The particle size, shapes, and the morphology of the WTR-SO_3H was studied by the SEM image, Fig. 1a. The SEM image revealed that the WTR-SO_3H consists of particles with a wide range of size with irregular shape. Most of the particles were measured to be micrometer in dimension.

The composition of the WTR-SO_3H was qualitatively and quantitatively determined by the EDS and SEM elemental mapping analyses,

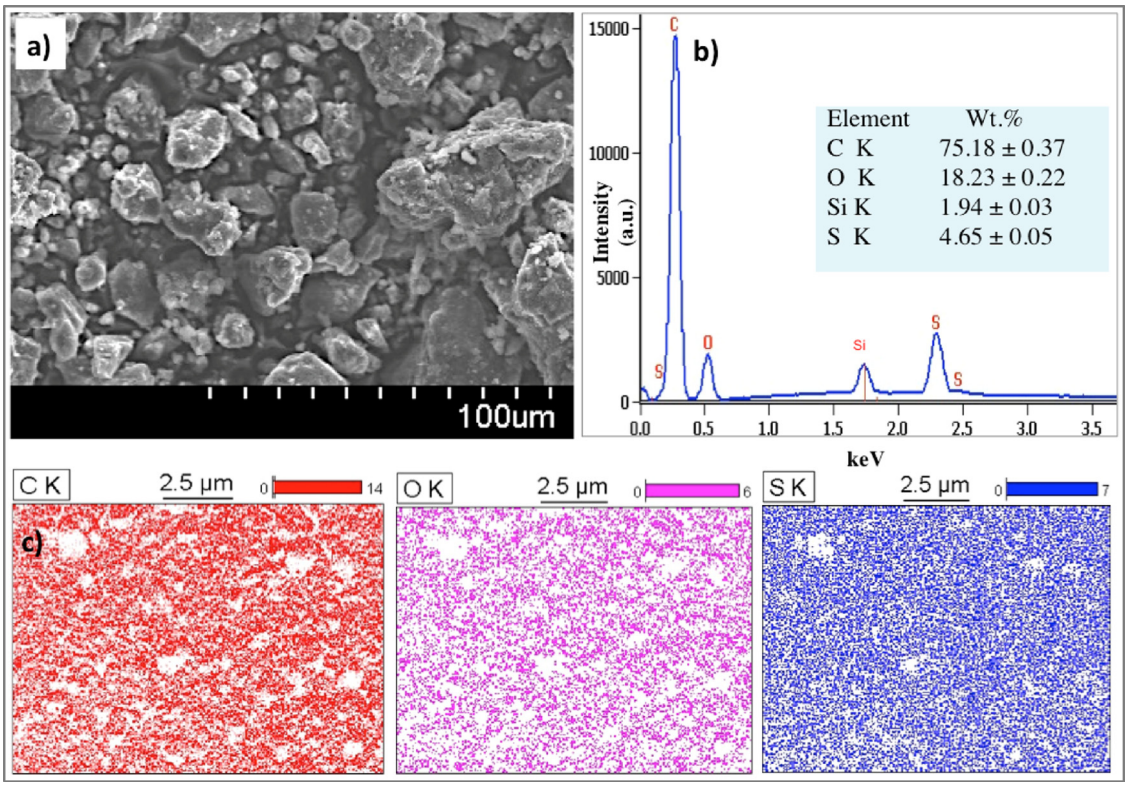

Fig. 1. a) SEM image of the WTR-SO_3H, b) EDS spectra showing the elemental composition of the WTR-SO_3H, and c) Elemental mapping image showing the presence of carbon, oxygen, and the sulfur in the WTR-SO_3H.

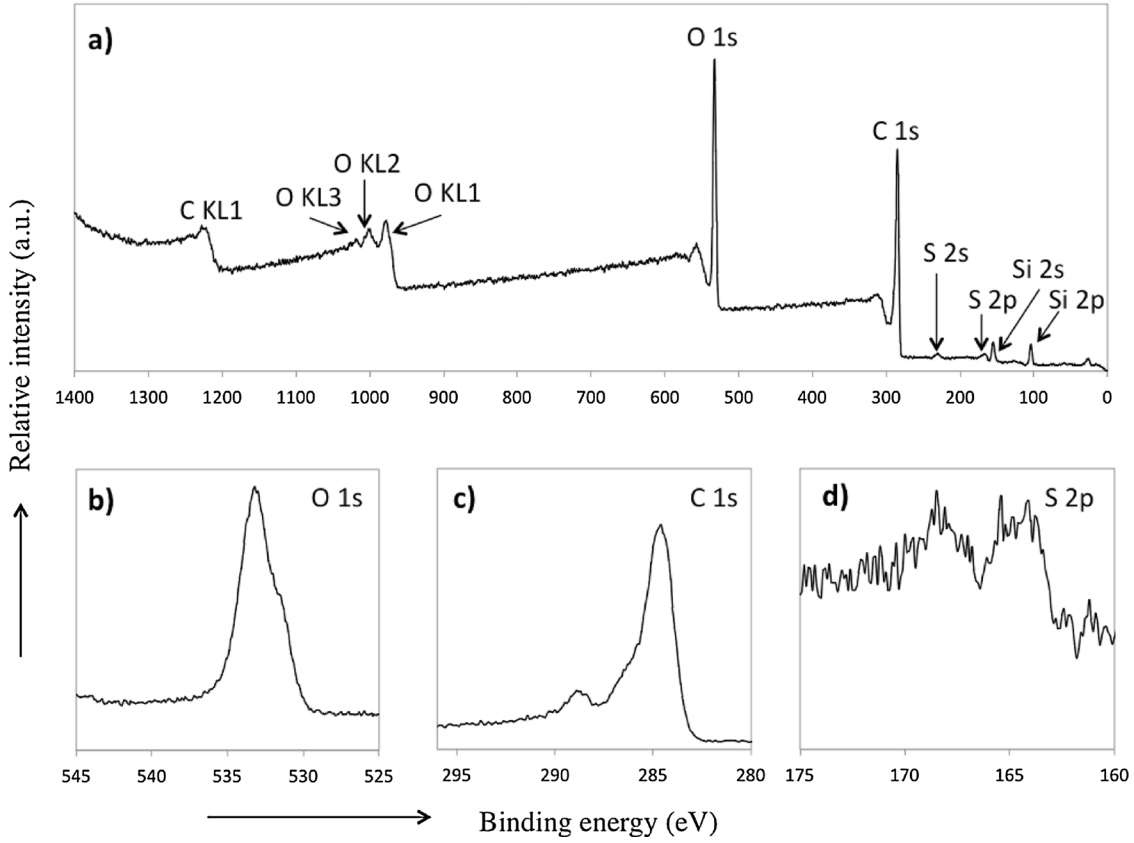

Fig. 2. a) XPS spectra of WTR-SO_3H. High-resolution XPS spectrum of b) O 1 s c) C 1 s and d) S 2p of the WTR-SO_3H.

Fig. 1b and c. The EDS spectrum and SEM elemental mapping confirmed that the WTR-SO_3H is chemically composed of carbon, oxygen, and sulfur. The presence of sulfur and oxygen further indicate the presence of $-SO_3H$ functional group, whereas the presence of carbon indicates the carbonaceous nature of the WTR-SO_3H. The approximate composition of the WTR-SO_3H, obtained from the EDS anaylsis, is shown in Fig. 1b (inset).

High resolution XPS was utilized to analyze the elemental composition and the functional groups of the WTR-SO_3H. The XPS spectra confirmed that the WTR-SO_3H is elementally composed of carbon, oxygen, and sulfur with silicon as the impurity, Fig. 2a. The S 2p3/2 and S 2p1/2 doublet with binding energies of about 164 eV could be assigned for the thiophenic group that is retained from the parent waste tire, Fig. 2d [31]. However, the S 2p3/2 and S 2p1/2 spin-orbital-split doublets observed at about 168 eV suggests the presence of sulfonic acid group (-SO_3H) [32–36]. Additionally, the presence of asymmetic O 1 s and C 1 s peaks, shown in Fig. 2b and c, supports the presence of sulfonic acid in the WTR-SO_3H [31,37,38].

The FTIR spectroscopy further confirmed the presence of different functional groups in the WTR-SO_3H, Fig. 3a. The presence of the C=C vibration of the sp^2 hybridized carbon skeleton could be indentified by the peaks at 1675 cm^{-1} and 1542 cm^{-1} [39]. The $-SO_3H$ functionl group was identified by the stretching vibration of S=O bond at ~1122, 1089, and 1005 cm^{-1} [40,41].

The degree of graphitization and imperfections in the WTR-SO_3H was examined by the Raman spectroscopy, Fig. 3b. Two bands located at ~1360 and 1582 cm^{-1} are attributed to the D and G bands, respectively. The D band indicates to the structural defect and disorder and the G band corresponds to the sp^2 carbon network in graphitic carbon [42–44]. In addition, the ratio of the intensities of the G to D band (ID/IG) is utilized to evaluate the extent of structural disorder for the WTR-SO_3H [45]. The ID/IG ratio for the WTR-SO_3H was found to be 1.015, which indicates that the WTR-SO_3H has high degree of defects and disorder [46]. Therefore, the FTIR, Raman, and the XPS studies suggest that the sulfuric acid treatment not only converted the waste tire rubber into the carbonaceous materials but also functionalized it by the sulfonic acid group.

X-ray powder diffraction spectroscopy (XRPD) was performed to further determine the crystalline and carbonaceous properties of the WTR-SO_3H, Fig. 3c. Two broad diffraction peaks located at ~24.78° and 42.17° could be indexed as the characteristic peaks originated from the (002) and (101) planes of amorphous carbon, respectively [47]. It was observed that (002) and (101) diffraction peaks of the WTR-SO_3H were slightly shifted to the left, in compared to the graphite (002) and (101) peaks (JCPDS Card No. 65e6212) [48,49]. Applying Bragg's equation ($n\lambda = 2d\sin\theta$), the lattice spacing (d in the Bragg's equation) of the WTR-SO_3H was calculated. It was found that the carbon in the WTR-SO_3H is somewhat extended from 3.356 Å to 3.588 Å along with (002) plane and 2.034 Å to 2.140 Å along with (101) plane [50].

The thermal stability and the decomposition profile of the WTR-SO_3H was detremined by carrying out the thermogravimetric analysis. As shown in Fig. 3d, the WTR-SO_3H loses the free and absorbed water in the molecular space from a temperature range from 50 to 250 °C. The major decomposition of the adsorbent started from about 325 °C and a complete decomposition of the WTR-SO_3H was observed at a temperature of about 600 °C and more. The TGA curve indicates that the WTR-SO_3H has very good thermal stability.

The pH-dependent zeta potential analysis was utilized to determine the net surface charge of the WTR-SO_3H in water, Fig. S2. The zeta potential gives important information to understand the mechanism of

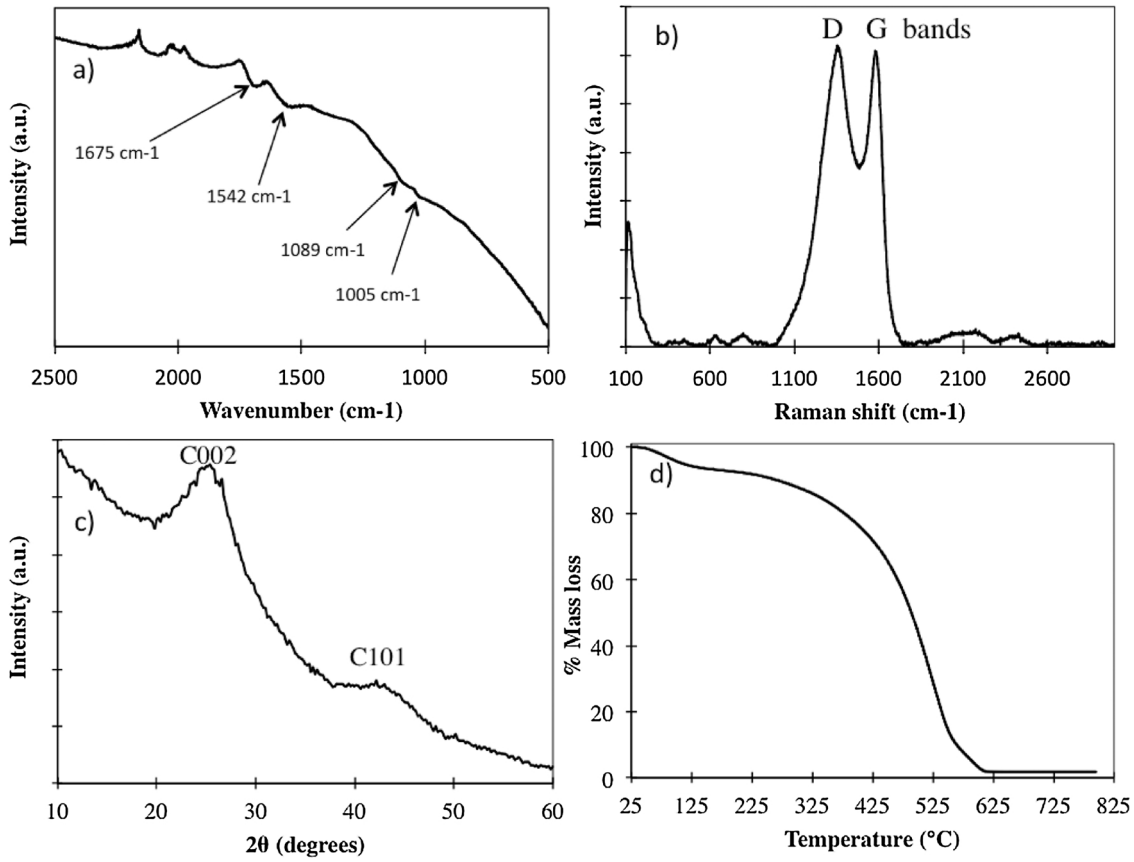

Fig. 3. a) FTIR spectra, a) Raman spectra, c) X-ray powder difffraction pattarn, and d) the thermal decomposition curve of the WTR-SO_3H.

adsorption by ionic interaction. It was found that the zeta potantial of the WTR-SO_3H in water is negative at a pH range of 1.5 to 11. Also, it could be observed that at a pH of 1.5, the negative zeta potential value is lowest and at pH 2.5 and above the negative zeta potential remains almost similar. The low pKa of the sulfonic acid (pKa ~ − 7) functional group suggests the WTR-SO_3H becomes sulfonate (WTR-SO_3^-) in water and thereby it gives negative zeta potential.

3.2. Effect of pH on the adsorption of MB, MO, and TC

The pH of the solution plays an important role in the adsorption efficiency as the zeta potential of the adsorbent and the net charge of the adsorbate change with the variation of the pH [51,52]. Therefore, the adsorption capacity of WTR-SO_3H for the MB, MO and TC was studied under a pH ranging from 3 to 10. The results demonstrate that the adsorption of MB increased with the increase in pH of the solution, Fig. 4a. MB is a basic dye, which stays positively charged when dissolved in water. Hence, in acidic pH the WTR-SO_3H surface becomes less negatively charged and thereby the adsorption by electrostatic attraction is retarded. With the increase in the solution pH the WTR-SO3H surface acquires negative charge (WTR-SO_3^-). Therefore, the adsorption of MB increases due to an increase in the electrostatic attraction between the positively charged dye (MB) and the negatively charged adsorbent (WTR-SO_3^-) [53]. Similar results were reported by

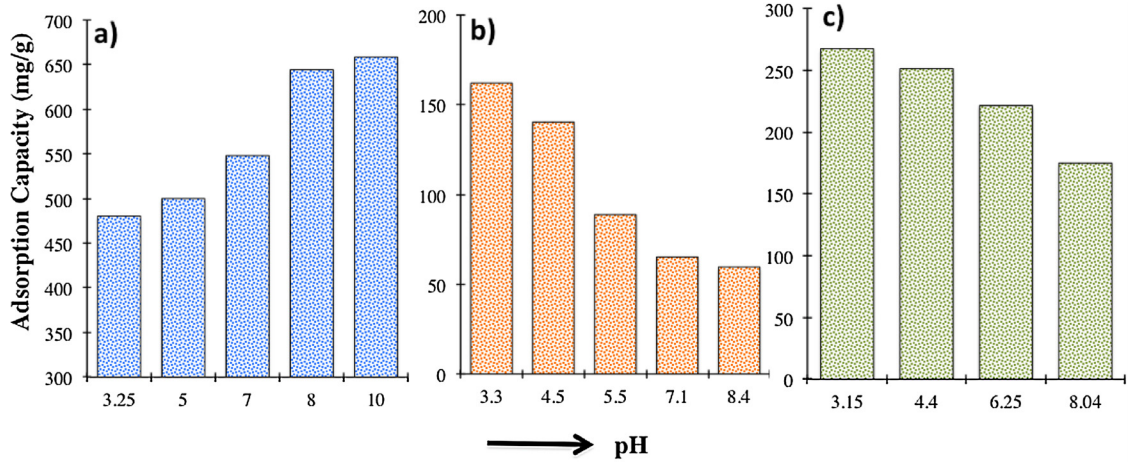

Fig. 4. The pH-dependent adsorption of a) MB, b) MO, and c) TC by the WTR-SO_3H, respectively. Initial MB concentration = 700 mg/L, V = 20 mL and adsorbent = 20 mg; initial MO concentration = 100 mg/L, V = 20 mL and adsorbent = 10 mg; initial TC concentration = 200 ppm, V = 20 mL and adsorbent = 10 mg.

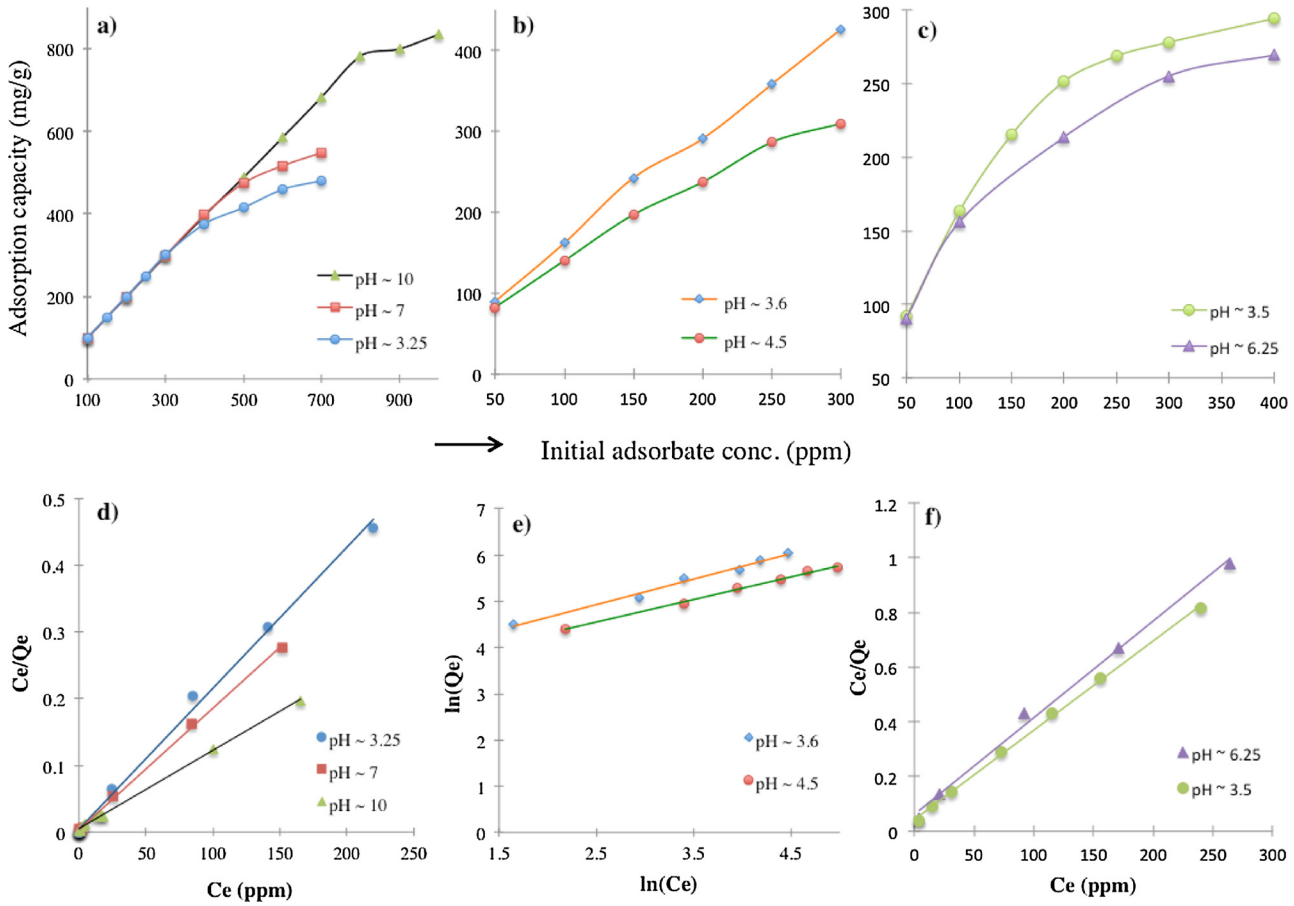

Fig. 5. Adsorption capacity of the WTR-SO_3H towards a) MB, b) MO, and c) TC at different initial adsorbate concentrations and pH. Linear form of the Langmuir (d& f) and the Freundlich (e) isotherm models for the adsorption of d) MB, e) MO, and f) TC.

other studies, where the adsorption of cationic dyes was favored at basic pH [54,55].

In contrast, the adsorption capacity for the MO and TC increased with the lowering of the pH, Fig. 4b and c. This effect is considered to happen due to the protonation of the amine functional groups of the MO and TC at the acidic pH. The electrostatic force of attraction between the ammonium group of the adsorbates and the sulfonate groups of the WTR-SO_3H bound them together. The results in agreement with the previously published researches [56,57].

3.3. Equilibrium adsorption capacity and the adsorption isotherms

The equilibrium adsorption capacity (Q_e), calculated by using Eq. (1), was found to increase with the increase in the initial pollutants concentration. The Q_e was calculated to be about 834 mg/g at an initial MB concentration of 1000 ppm and at pH ~10, Fig. 5a. For the adsorption of MO and TC, the Q_e was found to be 425 and 294 mg/g at the initial concentrations of 300 and 400 ppm, and the pH of 3.6 and 3.5, respectively, Fig. 5b and c. It was found that the Q_e for the adsorption of MB increased with the increase in the pH of the solution, whereas it is vice-versa for MO and TC. The unmodified waste tire rubber, on the other hand, showed negligible capacity for the MB, MO, and TC adsorption at pH 7, 3.6, and 3.5, respectively (Fig. S3). Therefore, it could be suggested that the sulfuric acid treatment converted the waste tire rubber into a high-capacity adsorbent for the removal of the MB, MO, and TC from water.

The linear form of the Langmuir, Freundlich, and Temkin isotherms were applied to the experimental data using Eqs. (3)–(5), respectively. Fig. 5d and f shows that the experimental adsorption data of MB and TC are in good fit with the Langmuir isotherm, which suggests that the adsorption of MB and TC happened by monolayer type adsorption. Applying the Langmuir isotherm equation (Eq. (3)), the maximum adsorption capacity (Q_m) of the WTR-SO_3H was calculated to be 833, 555, and 476 mg/g for MB at pH 10, 7 and 3.25, respectively. The Q_m for TC was calculated to be 303 and 285 mg/g at pH 3.5 and 6.25, respectively.

The Freundlich and Temkin adsorption isotherms (Eqs. (4) and (5)) were also applied on the experimental results for the adsorption of MB and TC. The experimental data of the MB adsorption were not in good fit with the Freundlich and Temkin isotherms, Fig. S4. However, the TC adsorption followed the Freundlich as well as the Temkin isotherms, Fig. S5, which suggests that the TC adsorption may have occurred by mono- and multilayer pattern.

The experimental data for the adsorption of MO was found to be in good fit with the linear form of the Freundlich isotherm, which suggests that the adsorption of MO happened by the multilayer pattern, Fig. 5e. The Langmuir and Temkin isotherm models were also applied and the correlation coefficients (R^2) values (Fig. S6) suggested that the adsorption of MO followed the Langmuir and Temkin models likewise the Freudnlich model. Therefore, applying the Langmuir isotherm equation (Eq. (3)), Q_m for MO was calculated to be 588 and 400 mg/g at pH 3.6 and 4.5, respectively.

3.4. Kinetics of adsorption

The time-dependent adsorption of MB, MO, and TC by the WTR-SO_3H is shown in Fig. 6. The results demonstrate a fast adsorption ability of the WTR-SO_3H and it was found that about 99% of the MB was adsorbed within 40 min, whereas for MO and TC it was about 80 and 90%, respectively after 100 min. The time-dependent adsorption

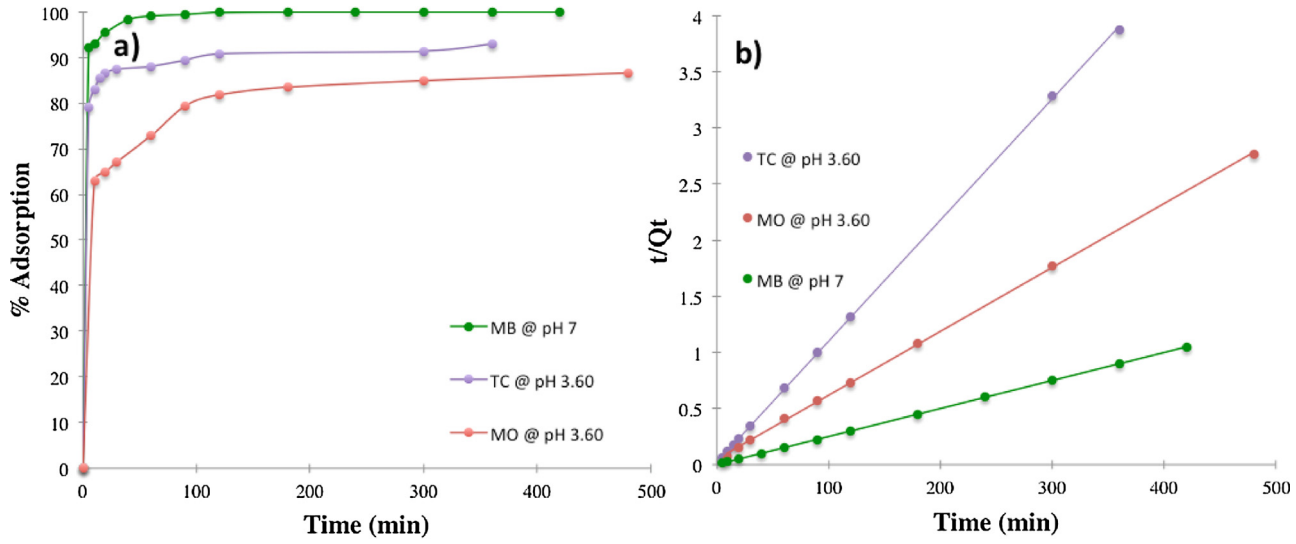

Fig. 6. a) Time-dependent adsorption of the MB, MO, and TC by the WTR-SO_3H; b) The pseudo-second-order kinetic model of the adsorption. Initial MB concentration = 200 mg/L, V = 40 mL and adsorbent = 20 mg; initial MO concentration = 100 mg/L, V = 20 mL and adsorbent = 10 mg; initial TC concentration = 50 mg/L, V = 20 mL and adsorbent = 10 mg.

capacity (mg/g) of MB, MO, and TC by the WTR-SO_3H is shown in Fig. S7.

Fig. 6b shows the linear form of the Pseudo-second-order kinetic model, which was obtained by using Eq. (6). For the adsorption of MB, MO and TC, the relationship between the t/Q_t vs. time was found to be linear having the values of correlation coefficients (R^2) equals 1. Moreover, the perfect fit of the Pseudo-second-order kinetic model suggests that the adsorption of MB, MO, and TC is favored by chemisorption. The values of Pseudo-second-order rate constants of MB, MO, and TC adsorption were calculated to be 1.471 and 3.25, 0.121, and 0.264 $g/mg^{-1}\,min^{-1}$, respectively.

Additionally, the Pseudo-first-order, intra-particle diffusion, and the Elovich kinetic models were applied to the time-dependent adsorption experimental data. However, the poor correlation coefficients of the linear fit suggested that the adsorption kinetics poorly followed the Pseudo-first-order, intra-particle diffusion, and the Elovich kinetic models, Fig. S8.

3.5. Thermodynamics of adsorption

Different thermodynamic parameters, such as the adsorption free energy, enthalpy and entropy changes were calculated for the adsorption of MB and MO over WTR-SO_3H. Fig. 7 shows the temperature-dependent adsorption capacity and their Langmuir isotherm plots at the temperature of 23, 40 and 60 °C. It was observed that the adsorption capacity for MB and MO decreased with the increase in the adsorption temperature, which suggests an exothermic adsorption process.

The Gibbs free energy change (ΔG) of adsorption was calculated using the following equation [58].

$$\Delta G = -RT\ln(K_L) \quad (10)$$

where R is the universal gas constant (8.31 $Jmol^{-1}\,K^{-1}$) and K_L is the Langmuir constant (L/mol), which can be obtained from the *slope/intercept* of the Langmuir plot, Fig. 8c and d.

The Gibbs free energy change (ΔG) for the adsorption of MB at temperature 23, 40, and 60 °C was calculated to be −7.88, −8.74, and −8.73 kJ/mol, respectively. The ΔG for the adsorption of MO at temperature 23, 40, and 60 °C was calculated to be −4.80, −6.67, and −6.90 kJ/mol, respectively. The negative values of the ΔG suggests the spontaneous adsorption of MB and MO on the WTR-SO_3H under the experimental conditions.

Additionally, the enthalpy and entropy changes (ΔH and ΔS) of adsorption was obtained using the van't Hoff equation [59].

$$\ln K_L = -\frac{\Delta H}{RT} + \frac{\Delta S}{R} \quad (11)$$

The ΔH values, calculated from the van't Hoff plot (Fig. 8), were −1101.65 and −673.1 J/mol for MB and MO, respectively. The negative values further confirmed the exothermic adsoprion process of MB and MO on the WTR-SO_3H.

The values of the entropy change ΔS were also obtained from the van't Hoff plot, Fig. 8. The ΔS values were calculated as +23.43, +4.30 $J/mol^{-1}\,K^{-1}$ for MB and MO, respectively. The positive values of the entropy changes suggests that the adsorption of the MB and MO are entropically favored. Therefore, applying the equation ($\Delta G = \Delta H - T\Delta S$) it could be concluded that the adsorption of MB and MO is enthalpically unfavored but entropically favored.

3.6. Adsorption of MB, MO, and TC from tap water

The adsorption capacity of the WTR-SO3H towards MO, MB, and TC was further determined from the tap water, Fig. 9. It was found that the adsorption capacity was weakly influenced by the coexisting ions present in tap water. The adsorption capacity towards MB was found to be 858 with 74% removal efficiency (Eq. (2)) at an initial MB concentration of 1200 ppm and pH 7. The equilibrium adsorption capacity towards TC was measured to be 232 mg/g at an initial TC concentration of 250 ppm with an unadjusted pH.

For the adsorption of MO, it was observed that MO could not be dissolved more than 25 ppm in tap water, which is because of the presence of metallic and nonmetallic ions in tap water. Therefore, the adsorption ability was measured by dispersing different amount of adsorbent to 25 mL of 25 ppm MO solution at pH ~ 3.6, Fig. 9c. The results show that 40 mg of the WTR-SO_3H adsorbed more than 99% of MO from the solution in tap water.

3.7. Adsorbent packed column for the continuous adsorption of MB and TC from tap water

The ability of the WTR-SO_3H towards the adsorption of MB and TC from tap water was further investigated under the continuous flow conditions. The column was used for three cycles for the adsorption of MB, Fig. 10. On the 1st cycle, the column efficiently filtered up to 26 Liters of 20 ppm MB solution from tap water, with a removal

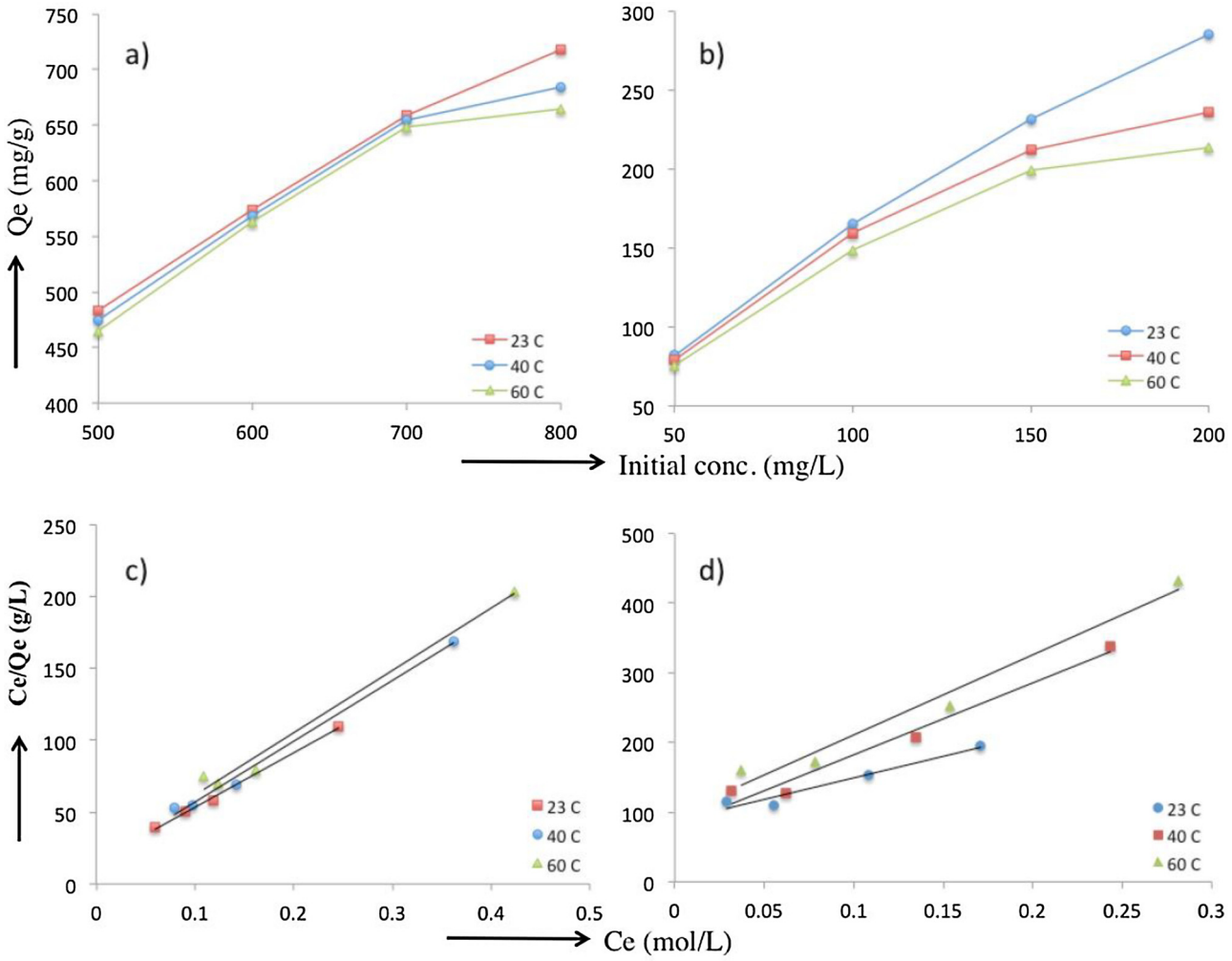

Fig. 7. Temerature-dependent adsorption capacity of the WTR-SO_3H for MB and MO at pH 10 and 3.6, respectively (a and b). Langmuir isotherm plot for the adsorption of MB and MO at different temperatur (c and d).

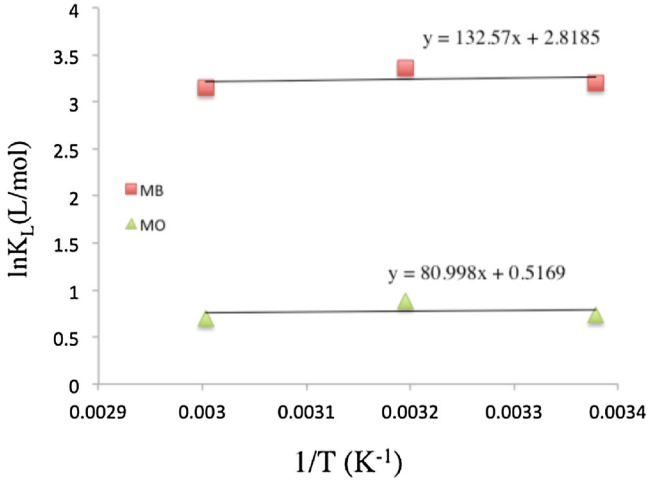

Fig. 8. Van't Hoff plots to obtain the ΔH and ΔS of the MB and MO adsorptions.

efficiency of ~98% at the end. However, on the 2nd and the 3rd cycle, the adsorption capacity of the column increased and it filtered up to 34 and 43 Liters of water with the removal efficiency of ~98% at the end, respectively. This happened after the column was regenerated with a mixture of reagent alcohol and water (99:1) with 0.025 M NaOH. A similar result was obtained during the filtration of TC in a separate column, which is discussed later. The continuous adsorption of TC was investigated at an unadjusted pH ~ 7.1 for the 1st cycle and pH ~ 3.5 the 2nd cycle, respectively. Acidic and basic pHs were chosen to investigate the pH-dependent adsorption capacity of the column. The column filtered up to 15 and 35 Liters of 10 ppm TC solution from tap water with the removal efficiency of 92% for the 1st and 2nd cycle, respectively. The increase in the adsorption capacity on the second cycle is assumed to happen because of the acidic pH of the feed TC solution, which is similar to the findings of the batch adsorption results. In the pH-dependent tests it was found that the acidic pH facilitated the adsorption of TC on the WTR-SO_3H.

To study the reason why the adsorption efficiency of the column increased after the regeneration with alkaline organic solvent, SEM image was taken on the WTR-SO_3H that was obtained from the MB column filter after all cycles of adsorption and regeneration, Fig. 11. The SEM image revealed that the regenerated WTR-SO_3H changed the morphology and exfoliated into a sponge like soft polymer in contrast to the fresh adsorbent, Fig. 1a. Also, it was observed that the particle size of the WTR-SO_3H decreased after the regeneration. The exfoliation and decrease in the particles size of the regenerated WTR-SO_3H probably happened because of the penetration of the organic solvent viz. reagent alcohol or acetone into the adsorbent and the electrostatic repulsion of the negative charges via the sulfonate groups of the adsorbent, which induced the polymer expansion by better solvation. A similar result was observed in our previous report [28].

Because of the more exfoliated morphology and smaller particles

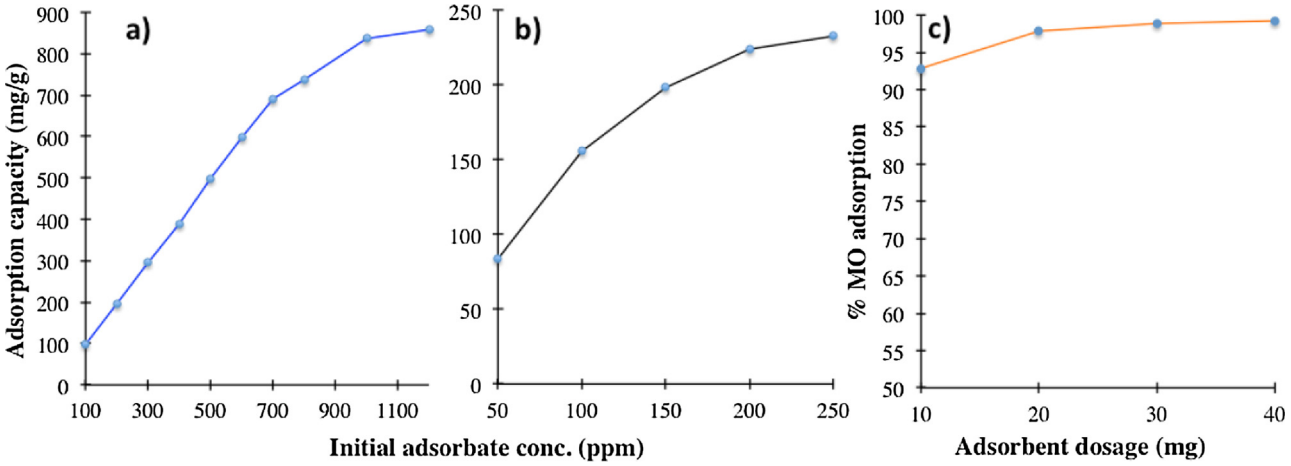

Fig. 9. Adsorption capacity of the WTR-SO_3H towards a) MB, b) TC and c) MO from tap water matrix.

size, the regenerated WTR-SO_3H obtained higher specific surface area and become more exposed to the adsorbate. As a result, we assume that the regenerated WTR-SO_3H exhibited higher adsorption capacity towards the MB in the column.

3.8. Suggested adsorption mechanism

Although detailed study is necessary to completely understand the adsorption of MB, MO, and TC on the WTR-SO_3H, a number of different interactions viz. ionic or electrostatic, π–π, hydrogen bonding, van-der-waals, hydrophobic interactions could be utilized to explain the adsorption process. The chemical structure of MB, MO, and TC consists of aromatic ring with different degree of conjugations, which favors their adsorption on the carbonaceous adsorbent by the π–π stacking interaction, Scheme 3. Moreover, MB has a flat extended conjugated structure, which has stronger π-π stacking interactions compared to the MO and TC. In addition, MB is a cationic dye, which exists as positively charged in aqueous solution. Therefore, MB gets adsorbed on the WTR-SO_3H surface by the electrostatic attractive forces between the negative charge of the sulfonate group of the WTR-SO_3H and the positive charge of the MB.

On the other hand, MO consists of two aromatic rings that are conjugated by a diazo (N═N) bond. There is a tertiary amine group on one benzene ring and a sulfonate group on the other benzene ring of the

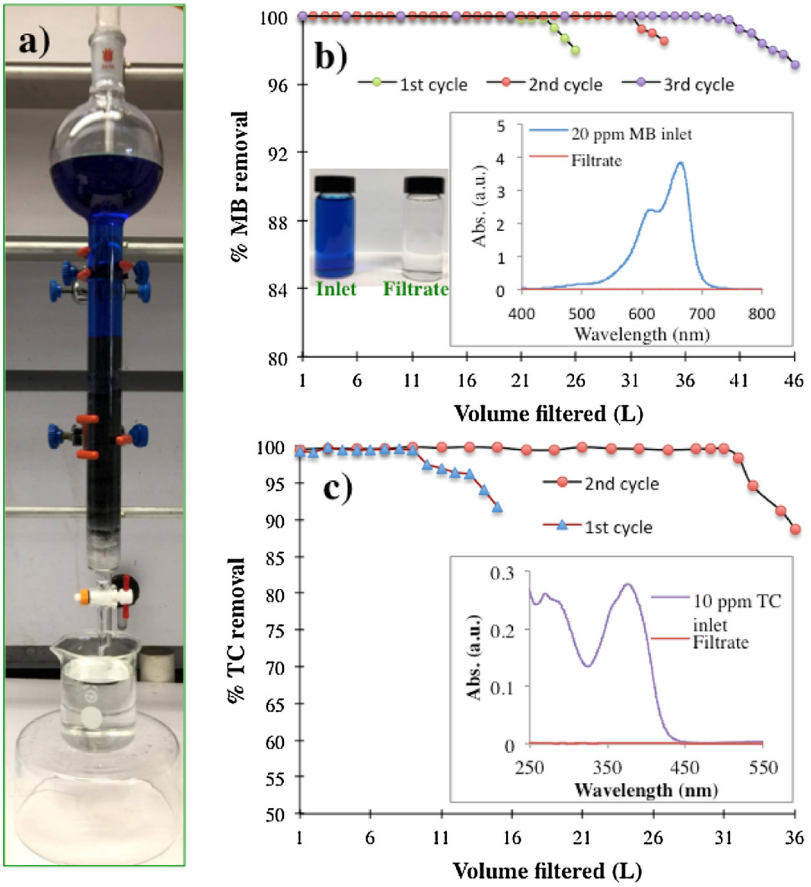

Fig. 10. a) An operating column packed with a mixture of WTR-SO_3H and sand, b) and c) percent MB and TC removal vs. the volume of the feed solution filtered through the column. Insets: UV–visible spectrum of the MB and TC in the feed and filtrate solutions.

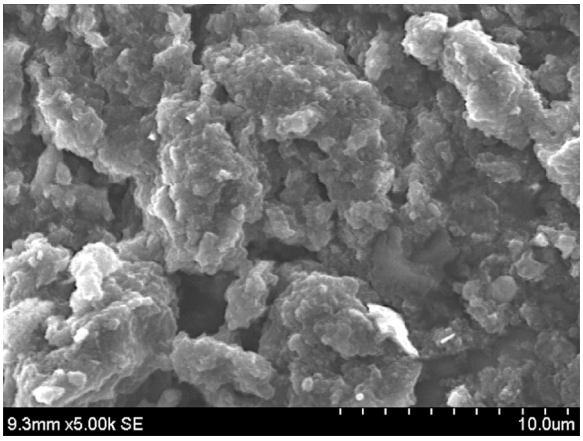

Fig. 11. Typical SEM image of the WTR-SO_3H obtained from the adsorbent column after all the adsorption and regeneration cycles.

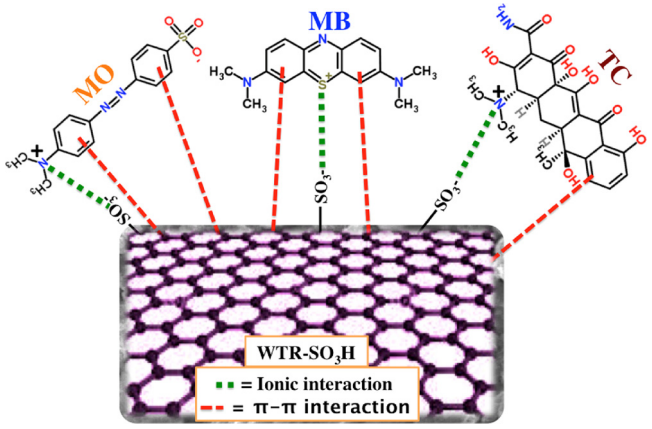

Scheme 3. Proposed mechanism for the adsorption of MB, MO, and TC over the WTR-SO_3H.

MO molecule. Therefore, at the acidic pH, MO can bind to the WTR-SO_3H by the π-π stacking as well as the ionic interaction between the sulfonate group of the adsorbent and the tertiary ammonium group of the MO. However, at basic pH the electrostatic repulsion between the sulfonate groups of the MO and the WTR-SO_3H hinders the adsorption. TC, on the other hand, has an aromatic ring with an extended conjugation system with various functional groups viz. phenol, alcohol, ketone, and tertiary amine and amide. At acidic pH < 3.3, TC becomes positively charged by the tertiary ammonium functional groups. Therefore, at acidic pH the TC adsorption is favored by the ionic interaction between the sulfonate group of the WTR-SO_3H and the tertiary ammonium group of the TC. In the pH range from 3.3 to 7.68, the TC becomes mostly zwitterionic. Therefore, the electrostatic interaction remains almost same in this range of pH and thereby the adsorption capacity remains also almost same. At basic pH > 8, the TC molecule becomes negatively charged by the phenolate and the hydroxylate functional groups, which favor the electrostatic repulsion with the sulfonate group of the adsorbent [60]. Therefore, a hindered adsorption results giving a lower adsorption capacity. The π-π stacking interaction between the benzene ring of the TC and the adsorbents also favors the adsorption.

3.9. Comparison of the adsorption capacities with other adsorbents

Table 1 shows the maximum adsorption capacity (Q_m) of the WTR-SO_3H in compared to various other adsorbents reported in the literature. It can be noticed that the adsorption capacity of the WTR-SO_3H towards MB, MO, and TC is higher than activated charcoal, carbon nanotube, graphene, graphene oxide and MOF-235. Therefore, the WTR-SO_3H could potentially be used as a low-cost and high-capacity adsorbent for the removal of MB, MO, and TC in the resource-limited areas.

Table 1
Comparison of adsorption capacities of various adsorbents for the removal of MB, MO and TC from deionized water.

Adsorbent (Pollutants)	Q_{max} (mg/g)	T(k)	pH	References
Activated charcoal (MB)	25	298	7	[61]
Graphene (MB)	153	293	7	[62]
MOF-235 (MB)	220	298	10.5	[63]
WTR-SO_3H (MB)	833	296	10	This work
WTR-SO_3H (MB)	555	296	7	This work
WTR-SO_3H (MB)	476	296	3.25	This work
Activated Carbon (MO)	300	298	7	[64]
Graphene oxide (MO)	17	298	3	[65]
MOF-235 (MO)	49	29	3.6	[63]
WTR-SO_3H (MO)	588	296	3.6	This work
WTR-SO_3H (MO)	400	296	4.25	This work
Bamboo charcoal (TC)	23.5	303	7	[66]
Graphene oxide (TC)	313	298	3.6	[67]
Carbon nanotubes (TC)	269	298	2.3	[68]
WTR-SO_3H (TC)	303	296	3.5	This work
WTR-SO3H (TC)	285	296	6.25	This work

4. Conclusion

The development of multifunctional adsorbents for the removal of organic pollutants in water using recycled materials may lead to new technologies with a sustainable economic and environmental impact in resource-limited areas. We reported a new high-capacity regenerable adsorbent derived from the rubber of used car tires transformed by the treatment of sulfuric acid. The adsorption ability of the adsorbent was evaluated with MB, MO, and TC, which are emerging environmental contaminants in water. Batch adsorption studies demonstrated that the adsorption is affected by various conditions such as solution pH, contact time, and the temperature. The maximum adsorption capacities were found to be 833 mg/g for MB, 555 mg/g for MO, and 303 mg/g for TC. The adsorption of MB, MO, and TC from tap water matrix was also performed and shown to maintain similar adsorption capacities. In conclusion, this work suggests that sulfuric acid treated waste tire material can potentially develop into a scalable, low-cost, high-capacity adsorbent for the removal of organic pollutants from water, thus promoting a new kind of synergism between pollutants used to treat other pollutants for sustainable environmental remediation.

Acknowledgements

Financial support from NSF grants ERC Nanotechnology-Enabled Water Treatment Center1449500, CHE-0748913, DMR PREM-1205302, and USDA2014-38422-22078 are gratefully acknowledged. We thank Dr. Gardea Torresdey research group for their kind assistance with the zeta potential experiments.

Appendix A. Supplementary data

Supplementary data associated with this article can be found, in the online version, at https://doi.org/10.1016/j.jece.2018.04.058.

References

[1] P.J. Van Beukering, M.A. Janssen, Trade and recycling of used tires in Western and Eastern Europe, Resour. Conserv. Recycl. 33 (2001) 235–265.
[2] S. Ramarad, M. Khalid, C.T. Ratnam, A.L. Chuah, W. Rashmi, Waste tire rubber in polymer blends: a review on the evolution: properties and future, Prog. Mater. Sci. 72 (2015) 100–140.

[3] V.K. Gupta, I. Ali, T.A. Saleh, M.N. Siddiqui, S. Agarwal, Chromium removal from water by activated carbon developed from waste rubber tires, Environ. Sci. Pollut. Res. 20 (2013) 1261–1268.
[4] H.Z. Mousavi, A. Hosseinifar, V. Jahed, Removal of Cu (II) from wastewater by waste tire rubber ash, J. Serb. Chem. Soc. 75 (2010) 845–853.
[5] S.J.T. Pollard, G.D. Fowler, C.J. Sollars, R. Perry, Low-cost adsorbents for waste and wastewater treatment: a review, Sci. Total. Environ. 116 (1992) 31–52.
[6] L.A. Sánchez-Olmos, J. Medina-Valtierra, K. Sathish-Kumar, M. Sánchez Cardenas, Sulfonated char from waste tire rubber used as strong acid catalyst for biodiesel production, Environ. Prog. Sustain. Energy 36 (2017) 619–626.
[7] Z.D. Hood, S.P. Adhikari, Y. Li, A.K. Naskar, L. Figueroa-Cosme, Y. Xia, M.P. Paranthaman, Novel acid catalysts from Waste-Tire-Derived carbon: application in Waste–to-Biofuel conversion, ChemistrySelect 2 (2017) 4975–4982.
[8] A.K. Naskar, Z. Bi, Y. Li, S.K. Akato, D. Saha, M. Chi, M.P. Paranthaman, Tailored recovery of carbons from waste tires for enhanced performance as anodes in lithium-ion batteries, RSC Adv. 4 (2014) 38213–38221.
[9] Y. Li, M.P. Paranthaman, K. Akato, A.K. Naskar, A.M. Levine, R.J. Lee, A. Manthiram, Tire-derived carbon composite anodes for sodium-ion batteries, J. Power Sources 316 (2016) 232–238.
[10] B.C. Yu, J.W. Jung, K. Park, J.B. Goodenough, A new approach for recycling waste rubber products in Li–S batteries, Energy Environ. Sci. 10 (2017) 86–90.
[11] N. Khatri, S. Tyagi, Influences of natural and anthropogenic factors on surface and groundwater quality in rural and urban areas, Front. Life Sci. 8 (2015) 23–39.
[12] S.K. Peddini, C.P. Bosnyak, N.M. Henderson, C.J. Ellison, D.R. Paul, Nanocomposites from styrene-butadiene rubber (SBR) and multiwall carbon nanotubes (MWCNT) part 1: morphology and rheology, Polymer 55 (2014) 258–270.
[13] R. Gong, J. Ye, W. Dai, X. Yan, J. Hu, X. Hu, H. Huang, Adsorptive removal of methyl orange and methylene blue from aqueous solution with finger-citron-residue-based activated carbon, Ind. Eng. Chem. Res. 52 (2013) 14297–14303.
[14] R. Acosta, V. Fierro, A.M. de Yuso, D. Nabarlatz, A. Celzard, Tetracycline adsorption onto activated carbons produced by KOH activation of tyre pyrolysis char, Chemosphere 149 (2016) 168–176.
[15] M.K. Liu, Y.Y. Liu, D.D. Bao, G. Zhu, G.H. Yang, J.F. Geng, H.T. Li, Effective removal of tetracycline antibiotics from water using hybrid carbon membranes, Sci. Rep. 7 (2017) 43717.
[16] Y. Gao, Y. Li, L. Zhang, H. Huang, J. Hu, S.M. Shah, X. Su, Adsorption and removal of tetracycline antibiotics from aqueous solution by graphene oxide, J. Colloid Interface Sci. 368 (2012) 540–546.
[17] J.E. Padilla, J. Melendez, L.A. Barrera, Y. Wu, K. Ventura, J.M. Veleta, J.C. Noveron, High dispersions of carbon nanotubes on cotton-cellulose benzoate fibers with enhanced electrochemical generation of reactive oxygen species in water, J. Environ. Chem. Eng. 6 (2018) 1027–1032.
[18] M.T. Islam, N. Dominguez, M.A. Ahsan, H. Dominguez-Cisneros, P. Zuniga, P.J. Alvarez, J.C. Noveron, Sodium rhodizonate induced formation of gold nanoparticles supported on cellulose fibers for catalytic reduction of 4-nitrophenol and organic dyes, J. Environ. Chem. Eng. 5 (2017) 4185–4193.
[19] I. Langmuir, The constitution and fundamental properties of solids and liquids, J. Am. Chem. Soc. 38 (1916) 2221–2295.
[20] H.M.F. Freundlich, Uber die adsorption in losungen, Zeitsch. Phys. Chem. 57 (1906) 385–470.
[21] R. Zhang, B. Wang, H. Ma, Studies on Chromium (VI) adsorption on sulfonated lignite, Desalination 255 (1–3) (2010) 61–66.
[22] K.Y. Foo, B.H. Hameed, Insights into the modeling of adsorption isotherm systems, Chem. Eng. J. 156 (1) (2010) 2–10.
[23] Y.C. Wong, Y.S. Szeto, W.H. Cheung, G. McKay, Equilibrium studies for acid dye adsorption onto chitosan, Langmuir 19 (2003) 7888–7894.
[24] A.H.M.G. Hyder, S.A. Begum, N.O. Egiebor, Adsorption isotherm and kinetic studies of hexavalent chromium removal from aqueous solution onto bone char, J. Environ. Chem. Eng. 3 (2015) 1329–1336.
[25] C. Duran, D. Ozdes, A. Gundogdu, H.B. Senturk, Kinetics and isotherm analysis of basic dyes adsorption onto almond shell (Prunus dulcis) as a low cost adsorbent, J. Chem. Eng. Data 56 (5) (2011) 2136–2147.
[26] P.K. Malik, Use of activated carbons prepared from sawdust and rice-husk for adsorption of acid dyes: a case study of Acid Yellow 36, Dyes Pigm. 56 (3) (2003) 239–249.
[27] M. Gouamid, M.R. Ouahrani, M.B. Bensaci, Adsorption equilibrium: kinetics and thermodynamics of methylene blue from aqueous solutions using date palm leaves, Energy Procedia 36 (2013) 898–907.
[28] M.T. Islam, C. Hernandez, M.A. Ahsan, A. Pardo, H. Wang, J.C. Noveron, Sulfonated resorcinol-formaldehyde microspheres as high-capacity regenerable adsorbent for the removal of organic dyes from water, J. Environ. Chem. Eng. 5 (2017) 5270–5279.
[29] O. Hamdaoui, Batch study of liquid-phase adsorption of methylene blue using cedar sawdust and crushed brick, J. Hazard. Mater. 135 (1–3) (2006) 264–273.
[30] Y. Li, Q. Du, T. Liu, X. Peng, J. Wang, J. Sun, et al., Comparative study of methylene blue dye adsorption onto activated carbon, graphene oxide, and carbon nanotubes, Chem. Eng. Res. Des. 91 (2) (2013) 361–368.
[31] Z.D. Hood, S.P. Adhikari, Y. Li, A.K. Naskar, L. Figueroa Cosme, Y. Xia, M.P. Paranthaman, Novel acid catalysts from waste tire derived carbon: application in Waste–to biofuel conversion, ChemistrySelect 2 (2017) 4975–4982.
[32] P. Siril, N. Shiju, D. Brown, K. Wilson, Optimising catalytic properties of supported sulfonic acid catalysts, Appl. Catal. A 364 (2009) 95–100.
[33] D.G. Castner, K. Hinds, D.W. Grainger, X-ray photoelectron spectroscopy sulfur 2p study of organic thiol and bisulfide binding interactions with gold surfaces, Langmuir 12 (1996) 5083–5086.
[34] H. Okawa, T. Wada, H. Sasabe, K. Kajikawa, K. Seki, Y. Ouchi, X-Ray photoelectron spectroscopy study of a self-assembled monolayer of thiophene thiol, Jpn. J. Appl. Phys. 39 (2000) 252.
[35] S.-A. Wohlgemuth, F. Vilela, M.-M. Titirici, M. Antonietti, A one-pot hydrothermal synthesis of tunable dual heteroatom-doped carbon microspheres, Green Chem. 14 (2012) 741–749.
[36] X.-L. Wei, M. Fahlman, A. Epstein, XPS study of highly sulfonated polyaniline, Macromolecules 32 (1999) 3114–3117.
[37] D.G. Castner, K. Hinds, D.W. Grainger, X-ray photoelectron spectroscopy sulfur 2p study of organic thiol and disulfide binding interactions with gold surfaces, Langmuir 12 (21) (1996) 5083–5086.
[38] X.L. Wei, M. Fahlman, A.J. Epstein, XPS study of highly sulfonated polyaniline, Macromolecules 32 (9) (1999) 3114–3117.
[39] M.A. Ishtiaque Shuvo, G. Rodriguez, M.T. Islam, H. Karim, N. Ramabadran, J.C. Noveron, Y. Lin, Microwave exfoliated graphene oxide/TiO2 nanowire hybrid for high performance lithium ion battery, J. Appl. Phys. 118 (12) (2015) 125102.
[40] T. Shen, C. Jiang, C. Wang, J. Sun, X. Wang, X. Li, A TiO 2 modified abiotic–biotic process for the degradation of the azo dye methyl orange, RSC Adv. 5 (2015) 58704–58712.
[41] F. Liu, S. Zuo, W. Kong, C. Qi, High-temperature synthesis of strong acidic ionic liquids functionalized, ordered and stable mesoporous polymers with excellent catalytic activities, Green Chem. 14 (5) (2012) 1342–1349.
[42] T. Jawhari, A. Roid, J. Casado, Raman spectroscopic characterization of some commercially available carbon black materials, Carbon 33 (1995) 1561–1565.
[43] M.A. Pimenta, G. Dresselhaus, M.S. Dresselhaus, L.G. Cancado, A. Jorio, R. Saito, Studying disorder in graphite-Based systems by raman spectroscopy, Phys. Chem. Chem. Phys. 9 (2007) 1276–1291.
[44] L.M. Malard, M.A. Pimenta, G. Dresselhaus, M.S. Dresselhaus, Raman spectroscopy in graphene, Phys. Rep. 473 (2009) 51–87.
[45] J. Ye, J. Zang, Z. Tian, M. Zheng, Q. Dong, Sulfur and nitrogen co-doped hollow carbon spheres for sodium-ion batteries with superior cyclic and rate performance, J. Mater. Chem. A. 4 (2016) 13223–13227.
[46] J. Ruan, T. Yuan, Y. Pang, S. Luo, C. Peng, J. Yang, S. Zheng, Nitrogen and sulfur dual-doped carbon films as flexible free-standing anodes for Li-ion and Na-ion batteries, Carbon 126 (2018) 9–16.
[47] Z. Qiu, Y. Lin, H. Xin, P. Han, D. Li, B. Yang, J. Xu, Ultrahigh level nitrogen/sulfur co-doped carbon as high performance anode materials for lithium-ion batteries, Carbon 126 (2018) 85–92.
[48] S. Peng, X. Fan, S. Li, J. Zhang, Green synthesis and characterization of graphite oxide by orthogonal experiment, J. Chil. Chem. Soc. 58 (2013) 2213–2217.
[49] Z. Ma, Y. Cui, X. Xiao, Y. Deng, X. Song, X. Zuo, A reconstructed graphite- like carbon micro/nano-structure with higher capacity and comparative voltage plateau of graphite, J. Mater. Chem. A. 4 (2016) 11462–11471.
[50] Q. Jiang, Z. Zhang, S. Yin, Z. Guo, S. Wang, C. Feng, Biomass carbon micro/nano-structures derived from ramie fibers and corncobs as anode materials for lithium-ion and sodium-ion batteries, Appl. Surf. Sci. 379 (2016) 73–82.
[51] S. Kaur, S. Rani, R.K. Mahajan, Adsorption kinetics for the removal of hazardous dye congo red by biowaste materials as adsorbents, J. Chem. 2013 (Article ID 628582).
[52] B.A. Fil, M. Korkmaz, C. Özmetin, Application of nonlinear regression analysis for methyl violet (MV) dye adsorption from solutions onto illite clay, J. Dispers. Sci. Technol. 37 (7) (2016) 991–1001.
[53] D. Pathania, S. Sharma, P. Singh, Removal of methylene blue by adsorption onto activated carbon developed from Ficus carica bast, Arab. J. Chem. 10 (2017) S1445–S1451.
[54] M.I. Khan, T.K. Min, K. Azizli, S. Sufian, H. Ullah, Z. Man, Effective removal of methylene blue from water using phosphoric acid based geopolymers: synthesis, characterizations and adsorption studies, RSC Adv. 5 (2015) 61410–61420.
[55] T. Jiao, Y. Liu, Y. Wu, Q. Zhang, X. Yan, F. Gao, B. Li, Facile and scalable preparation of graphene oxide-based magnetic hybrids for fast and highly efficient removal of organic dyes, Sci. Rep. 5 (2015).
[56] Y. Gao, Y. Li, L. Zhang, H. Huang, J. Hu, S.M. Shah, X. Su, Adsorption and removal of tetracycline antibiotics from aqueous solution by graphene oxide, J. Colloid Interface Sci. 368 (2012) 540–546.
[57] M.V. Subbaiah, D.S. Kim, Adsorption of methyl orange from aqueous solution by aminated pumpkin seed powder: kinetics, isotherms, and thermodynamic studies, Ecotoxicol. Environ. Saf. 128 (2016) 109–117.
[58] S. Wang, H. Li, L. Xu, Application of zeolite MCM-22 for basic dye removal from wastewater, J. Colloid Interface Sci. 295 (2006) 71–78.
[59] Z.-M. Ni, S.-J. Xia, L.-G. Wang, F.-F. Xing, G.-X. Pan, Treatment of methyl orange by calcined layered double hydroxides in aqueous solution: adsorption property and kinetic studies, J. Colloid Interface Sci. 316 (2007) 284–291.
[60] J. Jin, T. Feng, Y. Ma, W. Wang, Y. Wang, Q. Zhou, A. Li, Novel magnetic carboxyl modified hypercrosslinked resins for effective removal of typical PPCPs, Chemosphere 185 (2017) 563–573.
[61] M.J. Iqbal, M.N. Ashiq, Adsorption of dyes from aqueous solutions on activated charcoal, J. Hazard. Mater. 139 (2007) 57–66.
[62] T. Liu, Y. Li, Q. Du, J. Sun, Y. Jiao, G. Yang, Z. Wang, Y. Xia, W. Zhang, K. Wang, H. Zhu, Adsorption of methylene blue from aqueous solution by graphene, Colloids

Surf. B 90 (2012) 197–203.
[63] E. Haque, W.J. Jong, H.J. Sung, Adsorptive removal of methyl orange and methylene blue from aqueous solution with a metal-organic framework material, iron terephthalate (MOF-235), J. Hazard. Mater. 185 (2011) 507–511.
[64] K. Mahmoudi, N. Hamdi, A. Kriaa, E. Srasra, Adsorption of methyl orange using activated carbon prepared from lignin by $ZnCl_2$ treatment, Russ. J. Phys. Chem. A 86 (2012) 1294–1300.
[65] D. Robati, B. Mirza, M. Rajabi, O. Moradi, I. Tyagi, S. Agarwal, V.K. Gupta, Removal of hazardous dyes-BR 12 and methyl orange using graphene oxide as an adsorbent from aqueous phase, Chem. Eng. J. 284 (2016) 687–697.
[66] P. Liao, Z. Zhan, J. Dai, X. Wu, W. Zhang, K. Wang, S. Yuan, Adsorption of tetracycline and chloramphenicol in aqueous solutions by bamboo charcoal: a batch and fixed-bed column study, Chem. Eng. J. 228 (2013) 496–505.
[67] Y. Gao, Y. Li, L. Zhang, H. Huang, J. Hu, S.M. Shah, X. Su, Adsorption and removal of tetracycline antibiotics from aqueous solution by graphene oxide, J. Colloid Interface Sci. 368 (2012) 540–546.
[68] L. Zhang, X. Song, X. Liu, L. Yang, F. Pan, J. Lv, Studies on the removal of tetracycline by multi-walled carbon nanotubes, Chem. Eng. J. 178 (2011) 26–33.